David Taylor Research Center
Bethesda, MD 20084-5000

DTRC-90/003 January 1990

Ship Hydromechanics Department
Research and Development Report

A Design Method and an Application for Contrarotating Propellers

by
Benjamin Y.-H. Chen
Arthur M. Reed

Main text was presented at the
22nd American Towing Tank Conference,
St. John's, Newfoundland, Canada
8-11 August 1989.

MAJOR DTRC TECHNICAL COMPONENTS

CODE 011 DIRECTOR OF TECHNOLOGY, PLANS AND ASSESSMENT

12 SHIP SYSTEMS INTEGRATION DEPARTMENT

14 SHIP ELECTROMAGNETIC SIGNATURES DEPARTMENT

15 SHIP HYDROMECHANICS DEPARTMENT

16 AVIATION DEPARTMENT

17 SHIP STRUCTURES AND PROTECTION DEPARTMENT

18 COMPUTATION, MATHEMATICS & LOGISTICS DEPARTMENT

19 SHIP ACOUSTICS DEPARTMENT

27 PROPULSION AND AUXILIARY SYSTEMS DEPARTMENT

28 SHIP MATERIALS ENGINEERING DEPARTMENT

DTRC ISSUES THREE TYPES OF REPORTS:

1. **DTRC reports, a formal series,** contain information of permanent technical value. They carry a consecutive numerical identification regardless of their classification or the originating department.

2. **Departmental reports, a semiformal series,** contain information of a preliminary, temporary, or proprietary nature or of limited interest or significance. They carry a departmental alphanumerical identification.

3. **Technical memoranda, an informal series,** contain technical documentation of limited use and interest. They are primarily working papers intended for internal use. They carry an identifying number which indicates their type and the numerical code of the originating department. Any distribution outside DTRC must be approved by the head of the originating department on a case-by-case basis.

NDW DTNSRDC 5602 51 (Rev 2-88)

REPORT DOCUMENTATION PAGE

1a. REPORT SECURITY CLASSIFICATION: UNCLASSIFIED	1b. RESTRICTIVE MARKINGS
2a. SECURITY CLASSIFICATION AUTHORITY	3. DISTRIBUTION/AVAILABILITY OF REPORT: Approved for public release; distribution is unlimited.
2b. DECLASSIFICATION/DOWNGRADING SCHEDULE	
4. PERFORMING ORGANIZATION REPORT NUMBER(S): DTRC-90/003	5. MONITORING ORGANIZATION REPORT NUMBER(S):
6a. NAME OF PERFORMING ORGANIZATION: David Taylor Research Center; 6b. OFFICE SYMBOL (If applicable): Code 1544	7a. NAME OF MONITORING ORGANIZATION
6c. ADDRESS (City, State, and ZIP Code): Bethesda, Maryland 20084-5000	7b. ADDRESS (City, State, and ZIP Code)
8a. NAME OF FUNDING/SPONSORING ORGANIZATION: Office of Naval Technology; 8b. OFFICE SYMBOL (If applicable): Code 21	9. PROCUREMENT INSTRUMENT IDENTIFICATION NUMBER
8c. ADDRESS (City, State, and ZIP Code): 800 N. Quincy St., Arlington, VA 22217	10. SOURCE OF FUNDING NUMBERS: PROGRAM ELEMENT NO. 62121N; PROJECT NO. 4B401AB; TASK NO. RH21C10; WORK UNIT ACCESSION NO.

11. TITLE (Include Security Classification): A DESIGN METHOD AND AN APPLICATION FOR CONTRAROTATING PROPELLERS

12. PERSONAL AUTHOR(S): Chen, Benjamin Y.-H. and Reed, Arthur M.

13a. TYPE OF REPORT	13b. TIME COVERED	14. DATE OF REPORT (YEAR, MONTH, DAY)	15. PAGE COUNT
Final Report	FROM _____ TO _____	1990 January	33

16. SUPPLEMENTARY NOTATION: Main text was presented at the 22nd American Towing Tank Conference, St. John's, Newfoundland, Canada, 8—11 August 1989.

17. COSATI CODES			18. SUBJECT TERMS (Continue on reverse if necessary and identify by block number)
FIELD	GROUP	SUB-GROUP	Contrarotating Propellers, Interaction Velocities, Mass Conservation, Momentum Conservation, Circulation Conservation, Hub Effects

19. ABSTRACT (Continue on reverse if necessary and identify by block number)

A design methodology for contrarotating propellers has been developed based on rational hydromechanics. Three fundamental principles need to be satisfied: momentum, mass, and circulation conservation. Momentum conservation requires the net force generated by the contrarotating propeller to be balanced by the drag of the bare body and the drag due to hull-propulsor interaction. Mass conservation determines the circulation distribution of the aft propeller once the forward propeller circulation distribution is specified. Circulation conservation determines the magnitude of the circulation distribution of the aft propeller to ensure the proper thrust and torque ratios. The effects of the hub boundaries have been taken into account in the design and analysis methods. A contrarotating propeller set was designed for uniform flow at the operating point of the propeller for a high speed surface ship. Open water results show that the performance predictions agree well with the measurements.

20. DISTRIBUTION/AVAILABILITY OF ABSTRACT: ☒ UNCLASSIFIED/UNLIMITED ☐ SAME AS RPT ☐ DTIC USERS	21. ABSTRACT SECURITY CLASSIFICATION: UNCLASSIFIED	
22a. NAME OF RESPONSIBLE INDIVIDUAL: Benjamin Y.-H. Chen	22b. TELEPHONE (Include Area Code): (202) 227-1450	22c. OFFICE SYMBOL: Code 1544

DD FORM 1473, JUN 86 *Previous editions are obsolete.*

CONTENTS

FIGURES

FIGURES (Continued)

TABLES

NOMENCLATURE

c/D	Chord to diameter ratio
C_D	Drag Coefficient
C_f	Skin friction coefficient
CR	Contrarotating
C_{Th}	Thrust loading coefficient
D	Propeller diameter
EAR	Expanded area ratio
f_m/c	Maximum camber to chord length ratio
F	Ratio of forward propeller diameter to aft propeller diameter
G	Nondimensional circulation
i_t/D	Total rake to diameter ratio
K_Q	Nondimensional torque coefficient
K_T	Nondimensional thrust coefficient
LDV	Laser doppler velocimetry
N	Propeller RPM
P/D	Pitch to diameter ratio
Q	Torque
r	Nondimensional radius measured from the shaft axis
r_h	Nondimensional hub radius
R	Propeller radius
R_T	Total resistance
t	Thrust deduction factor
t/c	Thickness to chord ratio
T	Thrust
u_a	Axial induced velocity
$u_{a_{A,A}}, u_{a_{F,F}}$	Self-induced axial velocity for the aft and forward propellers, respectively
$u_{a_{A,F}}, u_{a_{F,A}}$	Axial velocity induced on the aft propeller by the forward propeller and vice versa
u_t	Tangential induced velocity
v_a	Axial inflow velocity
x	Axial separation between the forward and aft propellers
Z	Number of blades
β_i	Hydrodynamic pitch angle
Γ	Circulation
θ_S	Skew angle
ω	Angular velocity

Subscripts: F – Forward propeller
A – Aft propeller

All other notation in this report is in accordance with the International Towing Tank Conference (ITTC) Standard Symbols.*

* "International Towing Tank Conference Standard Symbols 1976," The British Ship Research Association, BSRA Technical Memorandum No. 500 (May 1976).

THIS PAGE INTENTIONALLY LEFT BLANK

A DESIGN METHOD AND AN APPLICATION FOR CONTRAROTATING PROPELLERS

Benjamin Y.-H. Chen and Arthur M. Reed

David Taylor Research Center, Bethesda, MD 20084, U. S. A.

ABSTRACT

A design methodology for contrarotating propellers has been developed based on rational hydromechanics. Three fundamental principles need to be satisfied: momentum, mass, and circulation conservation. Momentum conservation requires the net force generated by the contrarotating propeller to be balanced by the drag of the bare body and the drag due to hull-propulsor interaction. Mass conservation determines the circulation distribution of the aft propeller once the forward propeller circulation distribution is specified. Circulation conservation determines the magnitude of the circulation distribution of the aft propeller to ensure the proper thrust and torque ratios. The effects of the hub boundaries have been taken into account in the design and analysis methods. A contrarotating propeller set was designed for uniform flow at the operating point of the propeller for a high-speed surface ship. Open water results show that the performance predictions agree well with the measurements.

INTRODUCTION

Recently, there has been a renewed interest in finding more efficient replacements for current naval ship propulsion systems. One of the promising candidates is contrarotating (CR) propellers which exhibit many advantages over single screw propellers. These benefits are as follows:

1) Recovery of rotational energy that is normally lost in the slipstream.
2) Higher efficiency for a given disk area (i.e. smaller optimum diameter and lower loading per blade).
3) Increased cavitation inception speeds through reduced blade loading for blade surface cavitation and reduced circulation for tip vortex cavitation.
4) Torque balance resulting in simpler machinery mounting systems.

In spite of the hydrodynamic benefits of CR propellers, the application to surface ships has been limited because of the complex shafting and gearing arrangements required. Recently, interest in CR propellers has revived owing to the availability of lighter and more efficient electrical propulsion systems which provide CR propellers a new potential for application on surface ships.

Brief Review of CR propeller Design History

In the following, a brief chronicle of the development of CR propeller design technology is provided. In large, the survey is borrowed from Cox and Reed (1988). However, there are a few significant developments documented herein, which are not included in Cox and Reed.

Four decades ago, most of the research on CR propellers was experimental and design techniques were empirical. Since that time, analysis techniques based on the computer have been developed, so that today there are a number of sophisticated lifting-line and lifting-surface techniques available for use in propeller design.

One of the earliest theories for CR propellers was developed by Theodorsen (1944a, 1944b). Although his method was restricted to uniform flow, it showed that the analysis of CR propellers based on the ideal loading distribution for single propellers was inadequate. Naiman (1943) and McCormick (1953) included arbitrary assumptions concerning both the applicability of the Goldstein function and the orientation of the resulting induced velocities relative to the vortex sheets.

Lerbs (1955) developed the first lifting-line theory for CR propellers. He used the induction factors which he had previously derived for single rotation propellers (Lerbs 1952), so that the theory was released from the restrictions of empirical methods. Based on Lerbs' theory, Morgan (1960) developed a useable design technique for CR propellers. Relying on the assumption that the interference due to the lifting-surface effects between two propellers could be neglected, Morgan provided a detailed computational scheme for the design of optimum CR propellers. His paper also provided a detailed propeller design, accounting for cavitation and strength.

Based on momentum theory, Gunsteren (1971) developed a method for calculating the interaction effects between the two propellers. His approach provided a simple way for calculating the mutually-induced velocities and pressures. The radial distributions of the mutually induced velocities were calculated through lifting-line theory. He separated the self-induced velocities from the mutually-induced velocities so that each propeller could be treated as a single propeller.

Following Morgan's work, Caster and LaFone (1975) developed a second generation lifting-line design method. Using a lifting-line program for single screw propellers, Caster and LaFone uncoupled the circulation distribution for the forward and aft propellers. In addition, they incorporated field point velocity computations to determine the interaction velocities between the two propellers in an iterative procedure.

Nelson (1975) developed a series of computer programs for designing CR propellers which include: (1) A preliminary design program which can be used to perform parametric studies while the cavitation resistance is held constant. (2) A lifting-line program which can be used to perform the preliminary design. (3) A lifting-surface program which can be used to carry out the detailed design. In addition, Nelson (1972) presented a successful design method for CR propellers on torpedoes using circulation distributions with finite values at the blade roots. The methodology which he used is composed of lifting-line and lifting-surface methods.

In the early- to mid-1980's, Cox and Reed independently developed new lifting-line programs based on the Caster and LaFone method (Cox and Reed 1988). Both of the authors incorporated improved methods for computing the velocities induced by one propeller on the other. Cox also modified his lifting-line

method to incorporate finite loading at the hub and designed a CR propeller for uniform flow.

Chen and Reed (1988) developed a new lifting-surface program for CR propellers based on the MIT lifting surface design program with hub effects. This program automatically computes the velocities induced by one propeller on the other. In addition, the hub portion of the program has been modified to account for the velocities induced by one propeller on the other. The data from Laser Doppler Velocimetry (LDV) measurements of induced velocities were used to adjust the slope and distribution of the wakes which were shed from the two propellers.

Kerwin *et al.* (1986) developed the most recent lifting-line method for designing CR propellers. They employed variational methods to solve the two coupled lifting-line integro-differential equations simultaneously. Kerwin *et al.* used the vortex lattice approach to obtain a discrete representation of the circulation distribution in lieu of the traditional Fourier representation of the circulation distribution.

The purpose of the present study is to implement a design methodology for CR propellers using the principles of momentum, mass, and circulation conservation. The methodology incorporates finite loading at the blade roots into the design and analysis, and accounts for the effects of the hub boundary. The design methodology is implemented around the vortex lattice lifting-line theory developed by Kerwin *et al.* (1986) and as modified by Reed (Cox and Reed 1988); the lifting-surface theory of Greeley and Kerwin (1982) and as modified by Wang (1985) to account for hub effects; and the boundary element method of Lee (1987). A CR propeller set is designed for uniform flow at the operating point of the propeller for a typical high-speed surface ship. Force measurements for the CR propeller in uniform flow are given.

DESIGN METHODOLOGY FOR CR PROPELLERS

Design Principle

The fundamental principles which need to be satisfied in the CR propeller design are momentum, mass, and circulation conservation. Momentum conservation requires the net force generated by the CR propeller to be balanced by two kinds of drag: one is the drag of the bare body and the other is the drag due to the propeller-hull interaction. There are two phenomena which contribute to propeller-hull interaction: thrust deduction and wake fraction. Only thrust deduction, an additional drag, affects the momentum conservation. Thrust deduction is caused by the propeller accelerating the local flow field about the ship, resulting in a reduction of the hull pressures. The higher velocity also increases the wall shear stress, and hence, the frictional resistance. The thrust deduction factor for propellers is defined by:

$$1 - t = \frac{R_T}{T},$$

where R_T is the bare-hull resistance and T is the total thrust for all propellers.

Mass conservation determines the circulation distribution of the aft propeller once the circulation distribution of the forward propeller is specified. Based on this mass conservation, the preliminary diameter of the aft propeller can be determined by using the following formula:

$$R_A = F R_F, \qquad (1)$$

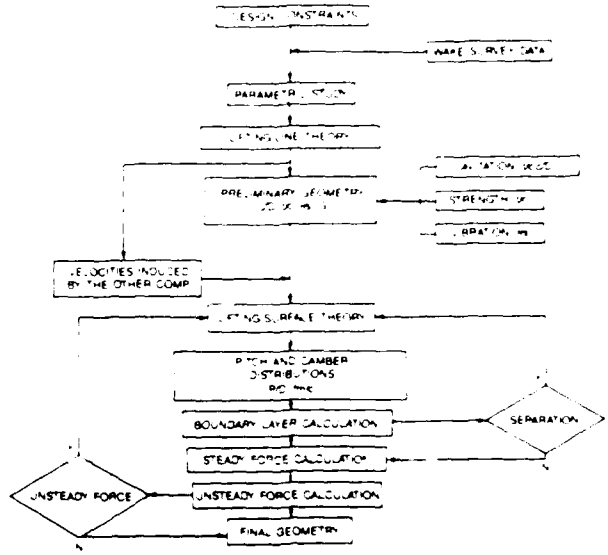

Fig. 1. Flow chart of CR propeller design methodology.

where

$$F = \left\{ \frac{\int_{r_{h_F}}^{1} dr r(v_{a_F} + u_{a_F F} + u_{a_F A})}{\int_{r_{h_A}}^{1} dr r(v_{a_A} + u_{a_A A} + u_{a_A F})} \right\}^{1/2}$$

The quantities v_{a_F} and v_{a_A} are the axial inflows for the forward and aft propellers, $u_{a_F F}$ and $u_{a_A A}$ are the axial self-induced velocities, $u_{a_F A}$ and $u_{a_A F}$ are the axial mutual interaction velocities induced at the forward and aft propeller planes, r is the local nondimensional radius of the propeller, and r_{h_F} and r_{h_A} are the hub radii of the forward and aft propellers, respectively.

The basic guideline for determining the final aft propeller diameter is to ensure that the tip vortices generated by the forward propeller blades will not impinge on the aft propeller blades. To be on the safe side, the final aft propeller diameter should be selected so as to be smaller than the preliminary aft propeller diameter using mass conservation without sacrificing too much efficiency.

Circulation conservation determines the magnitude of the aft propeller circulation to ensure proper thrust and torque ratios. In other words, once the magnitude of the forward propeller circulation is specified, the magnitude of the aft propeller circulation has to be calculated so as to conserve the total circulation.

Design Procedure

A flow chart of the design methodology for CR propellers is shown in Figure 1. It consists of three phases: operating conditions, design, and analysis.

In the first phase, the design requirements and the wake survey data need to be provided. The effects of hull on the flow and hull propulsor interaction are traditionally represented by the nominal wake and two interaction coefficients: the thrust deduction factor and the wake fraction. Although this design method is

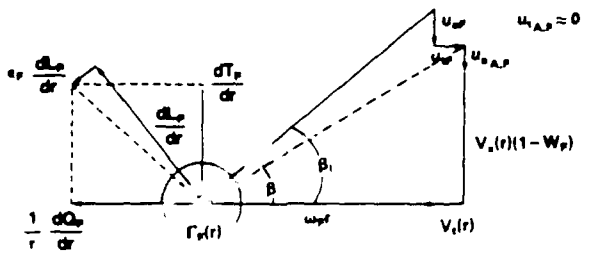

FORWARD PROPELLER (RIGHT-HANDED)

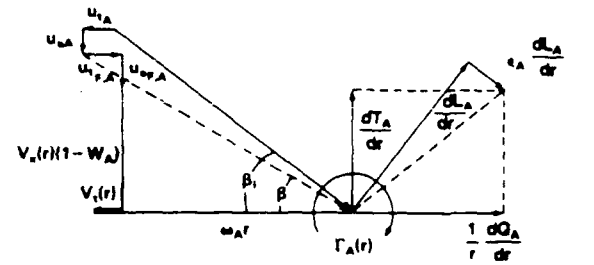

AFT PROPELLER (LEFT-HANDED)

Fig. 2. Velocity diagram for a CR propeller set.

general, and treats thrust deduction and circumferential-average wake distributions in the presence of a hull, in the following we restrict our consideration to uniform flow in the absence of a hull.

For this simple flow, we are immediately ready to start the second stage, the design stage. As was mentioned in the introduction, the traditional lifting-line design of CR propellers has been performed by coupling single screw propeller codes in an iterative process. Kerwin *et al.* (1986) developed a more advanced lifting-line theory for CR propellers. They used the vortex lattice method to solve the lifting-line problem for a CR propeller directly. The induced velocities in their theory include the self-induced velocities of each component as well as the velocities induced by the other component. A velocity diagram for the forward propeller (rotating at angular velocity ω_F) and aft propeller (rotating at angular velocity ω_A) of a CR propeller set is given in Figure 2.

The optimum circulation distribution in Kerwin *et al.*'s theory incorporates finite loading at the blade roots which is an important factor for CR propellers. The theory automatically provides equal and opposite total circulation for the forward and aft propellers at the hub, which insures minimum hub vortex strength, i.e., zero net circulation for the two propellers at the hub. In the present design procedure, the effects of the hub boundaries have been taken into account. In addition, the slope of the circulation, $d\Gamma/dr$, is constrained to be zero at the hub so that the trailing vortex sheet near that region is eliminated.

A comparison of the Lerbs' optimum circulation distributions for a single rotation propeller between Kerwin *et al.* (1986) and Caster *et al.* (1975) was given in Chen *et al.* (1988). The circulation distribution from Kerwin *et al.*'s program agrees very well with that from Caster *et al.*. This indicates that the variational method is a correct approach to lifting-line theory. However, it does not prove that Kerwin *et al.*'s program is correct for CR propellers. It must still be validated, which is is one of the purposes of the present study.

Due to the temporal and spatial variations in the velocity field in which the forward and aft propellers operate, the mutual interaction velocities between the two components are an unsteady flow both in space and time. However, a methodology which can handle these circumferential variations in the mutual interaction velocities for CR propellers is not necessary because of the fact that the design problem is solved for the circumferential average flow. Calculation of the circumferential-average mutual interaction velocities is one of the most critical factors affecting CR propeller design. Chen and Reed (1988) showed that the use of the interaction velocities calculated from lifting-line theory is adequate for lifting-surface design as long as the propeller loadings are moderate and the propellers are not too close to each other. Therefore, in the present study, the mutual interaction velocities from lifting-line theory have been used to simplify the lifting-surface design.

In the intermediate design stage, cavitation and strength are the major concerns. Blade surface cavitation can cause blade erosion, noise, and thrust loss which are detrimental to ship performance. In order to improve the cavitation performance, one can vary blade thickness, chord distribution, and blade loading. However, the strength and the propulsive performance are also affected by varying the above parameters.

The propeller is subjected to both hydrodynamic and centrifugal loadings as it operates. A propeller blade must contain enough material to keep the stress within a blade below a certain predetermined level. This acceptable stress level is a function of the material properties with regard to both steady state loading and fatigue strength, and to both the mean and unsteady blade loadings. Chord length, thickness, skew, and rake are the important propeller geometric parameters which will affect the stress. Based on the simple beam theory, the stress can be calculated by representing the propeller blade as a straight cantilever beam with variable cross section without camber. To have a more accurate analysis for the full power ahead case and the backing case, a finite element analysis is required.

In the final design stage, the detailed blade geometry (pitch and camber distributions) is determined using a lifting-surface theory which incorporates three-dimensional flow field effects. In the present study, a lifting-surface theory with hub-image effects developed by Wang (1985) is employed. The vortex lattice representation is adapted for the blades and their wakes. The hub is represented by a distribution of dipoles which ends at the hub apex. The dipole distribution allows non-zero circulation at the hub of a propeller, and allows the normal velocity at the hub to be zero.

All the design codes used in this effort are based on potential flow theory. The effect of viscous drag has been accounted for in the force calculations using the following empirical formula:

$$C_D = C_f[1 + 1.25(t/c) + 125(t/c)^4],$$

where C_f is the skin friction coefficient for a smooth plate, and t/c is the section thickness to chord ratio. The value of C_f varies from 0.008 down to 0.004 for blade-section Reynolds numbers varying between 10^6 and 10^8.

To ensure unseparated flow along the blade, boundary layer calculations need to be performed. In the present study, a program developed by Cebeci (1978) was employed. This program

has the capability to calculate incompressible laminar and turbulent boundary layers on plane and axisymmetric bodies with either smooth or rough surfaces.

During this phase of the design, steady forces and unsteady forces and moments also need to be calculated. To determine the steady thrust, torque, and efficiency of the CR propeller under design and off-design operating conditions, both a vortex-lattice method and a panel methods have been utilized in the present study; one is the vortex-lattice method developed by Greeley and Kerwin (1982) and the other is a potential-based panel method developed by Lee (1987).

Greeley and Kerwin solved the lifting-surface theory using a vortex lattice and line source representation of the blade, with the singularities placed on the mean camber surface. Lee adopted a surface panel method and distributed dipole panels on the exact propeller surface as well as the hub surface, which is significant for propellers with a large hub radius or a small number of blades. In addition, Lee used a pressure Kutta condition, which requires that the pressure on the upper and lower surfaces at the trailing edge be equal. Due to the nonlinearity of the pressure Kutta condition, an iterative process must be employed to solve for the three-dimensional trailing edge flow.

A CR PROPELLER DESIGN

In this section, a design is developed using the methodology described in the previous section. Some of the design stages will be skipped because the present design is for uniform flow.

Design Requirements

The CR propeller set was designed for uniform flow at the operating condition of a high-speed surface ship. The ship speed was chosen as 20.0 knots (10.3 m/sec). The forward propeller diameter was restricted to 6.1 meters and the rotational speed to 51 rpm. The blade numbers of the forward and aft propellers are 7 and 5, respectively. The ratio of the torque of the forward propeller to that of the aft propeller has to be maintained at 1.07 due to machinery constraints. This CR propeller design was constrained to produce the same thrust loading coefficient in uniform flow, a C_{TA} of 0.5849, as would be required in the hull wake.

The design parameters for the present study were chosen based on a parametric study. The aft propeller diameter was determined through mass conservation as shown in Equation 1. To ensure that the aft propeller operates inside the tip vortices of the forward propeller, the final aft propeller diameter, which is 85 percent of the forward propeller diameter, was chosen to be slightly smaller than the preliminary one calculated using mass conservation. The rotational speed of the aft propeller is 51 rpm which is identical to that of the forward propeller. The axial spacing was chosen as 0.25 of the forward propeller diameter. A summary of the design parameters for the CR propeller is given in Table 1.

Preliminary Design

The lifting-line calculations will be discussed in this section. The optimum circulation distributions for the forward and aft propellers are determined by the variational approach described in the previous section. Figure 3 presents the optimum circulation distributions for the forward propeller with and without hub effects. The circulation distribution accounting for the hub effects shows that maximum loading occurs at the blade roots while that without hub effects has zero loading at the hub. Additionally, the tip loading of the circulation distribution with hub effects is slightly smaller than that without.

Table 1. Contrarotating propeller design—summary

	Forward Propeller	Aft Propeller
N, rpm	51	51
C_{TA}	0.5849	
Geometry		
Diameter, m	6.096	5.182
Number of Blades	7	5
Expanded Area Ratio	0.632	0.507
Axial Spacing, m	1.524	
Skew, deg	25.0	25.0
Blade Sections	*	*

* NACA 66 (TMB Modified) Thickness, NACA $a = 0.8$ Meanline

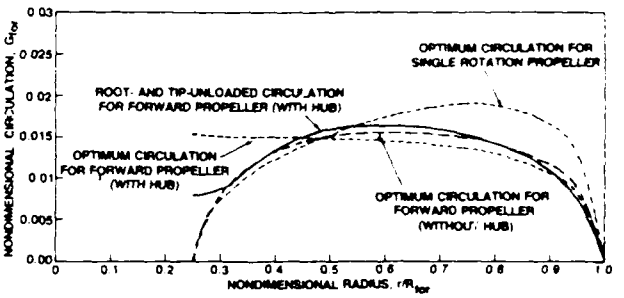

Fig. 3. Circulation distributions for forward propeller and single rotation propeller..

The optimum circulation distribution for a single rotation propeller in uniform flow is also illustrated in Figure 3. In contrast to the single rotation propeller blade loading, the forward propeller blade loading is shifted inboard so that the axial kinetic energy losses can be reduced. In addition, the magnitude as well as the slope of the blade loading at the tip of the forward propeller of the CR set are reduced, resulting in a projected improvement in the tip vortex cavitation inception speed.

The optimum and the root- and tip-unloaded circulation distributions for the forward propeller are also shown in Figure 3. The advantage of unloading the blade root is to delay the blade root cavitation inception and to reduce the tendency toward cavitation erosion near the blade root. Since the lift coefficient at the blade root is very high with the optimum circulation distribution, a 50-percent reduction in the blade loading at the root was made to lower the lift coefficient to less than 0.5. In addition, the slope of the circulation, $d\Gamma/dr$, is constrained to be zero at the blade root to eliminate the trailing vortex sheet. Similarly, the blade tip is unloaded to delay tip vortex cavitation inception and to reduce cavitation erosion at the tip. However, unloading the blade tip results in a reduction in propeller efficiency. Since the magnitude and slope of the blade loading at the tip of the forward propeller are much smaller than those of the single rotation propeller, a loading of 95 percent of the optimum loading at the 0.95 radii was chosen, so as to not sacrifice too much propeller efficiency.

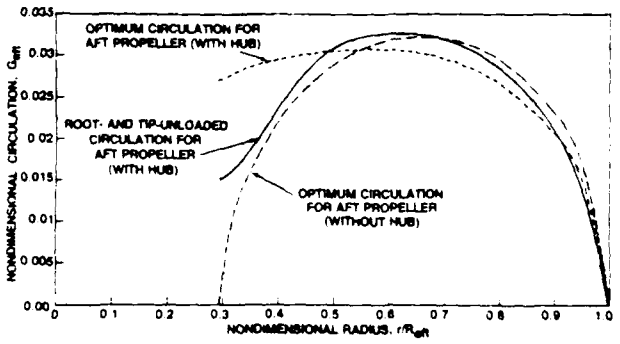

Fig. 4. Circulation distributions for aft propeller.

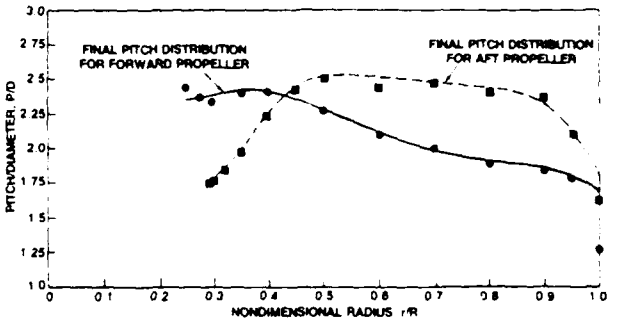

Fig. 5. Final pitch to diameter ratio distributions.

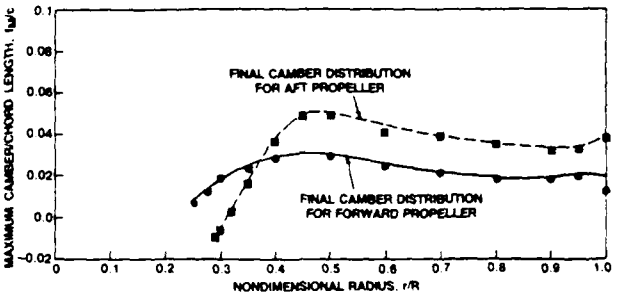

Fig. 6. Final maximum camber to chord length ratio distributions.

Figure 4 shows the optimum circulation distribution for the aft propeller with and without hub effects. As was shown for the forward propeller, the optimum circulation distribution for the aft propeller with hub effects has a higher circulation near the hub and lower circulation near the tip than the distribution without a hub.

The distributions of the optimum and root- and tip-unloaded circulations for the aft propeller are also given in Figure 4. The guideline for unloading the aft propeller hub has to consider two factors; one is to provide an equal and opposite total circulation at the hub with respect to the forward propeller to ensure zero hub vortex strength, and the other is to maintain zero circulation slope at the hub to eliminate the trailing vortex sheet. The loading at the hub was reduced by 50 percent to reduce the section lift coefficient to less than 0.5.

The chord-length distributions of the forward and aft propellers were chosen based on cavitation, flow separation, and efficiency considerations. The thickness distribution was selected based on strength and cavitation considerations.

A skew distribution with 25 degrees tip skew varying linearly from zero at the hub was selected for both propellers. The total rake for both propellers was zero. Thus, both propellers have negative rake to offset the skew-induced rake.

Intermediate Design

In the intermediate design stage, strength and cavitation are normally discussed. The stress distributions for the forward and aft propellers were calculated and were determined to be well below the allowable stress of 12,500 psi for Nickel-Aluminum-Bronze. Since this propeller set is designed for uniform flow, detailed cavitation predictions were not carried out for this design.

Final Design

The final pitch and camber distributions were determined using lifting-surface theory with hub effects included. A chordwise loading distribution corresponding to that of an a equals 0.8 mean line was employed on the blade sections. This decision was based on cavitation and viscous flow considerations. For this application, a NACA 66 thickness distribution was selected. Figures 5 and 6 show the respective final pitch and camber distributions for the forward and aft propellers. A solid model rendering of the CR propeller set generated on a *Computer Vision* system is shown in Figure 7.

Performance Prediction and Open-Water Tests

Aluminum models of the forward and aft propellers (DTRC Propellers 5067 and 5068) were manufactured based on the final design geometry. The propellers were tested in open water as a CR propeller set.

Figure 8 shows the experimental thrust coefficient, torque coefficient, and efficiency for the CR propellers (operating as a unit) as a function of advance coefficient; as well as the performance prediction at the design advance coefficient. Table 2 shows the predicted and measured performance of the CR propellers. At constant C_{Th}, the forward propeller thrust prediction is 2.3 percent higher than the experimental measurement. However, the aft propeller thrust is 3.1 percent lower. The forward and aft propeller torque predictions are 3.0 percent and 2.9 percent lower than their respective experimental measurements.

The design advance coefficient is 0.3 percent higher than the experimental measurment at the design C_{Th}. The unit thrust prediction is almost identical to the experiment and the unit

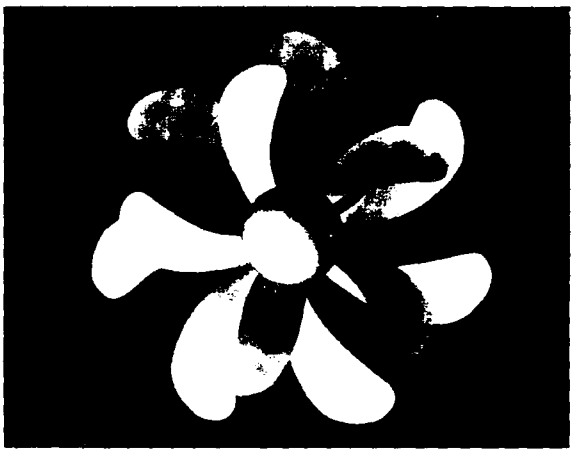

Fig. 7. Final geometry of CR propeller set.

Table 2. Predicted and measured performance of design contrarotating propellers operating as a unit.

	Design	Experiment
Forward Prop		
K_T	0.307 (+2.3%)	0.300
K_Q	0.0995 (−3.0%)	0.1026
η^*	0.780 (+5.7%)	0.737
Aft Prop**		
K_T	0.268 (−3.1%)	0.276
K_Q	0.0931 (−2.9%)	0.0959
η^*	0.728 (+0.3%)	0.726
Unit**		
J_S	1.589 (+0.3%)	1.584
K_T	0.575 (−0.1%)	0.576
K_Q	0.1926 (−3.0%)	0.1985
T_F/T_A	1.146 (+5.6%)	1.085
Q_F/Q_A	1.068 (+0.2%)	1.070
n_F/n_A	1.000	1.000
η^*	0.755 (+3.0%)	0.732

* $\eta = \frac{K_T J_S}{2\pi K_Q}$

** All nondimensional coefficients are based on the forward propeller diameter

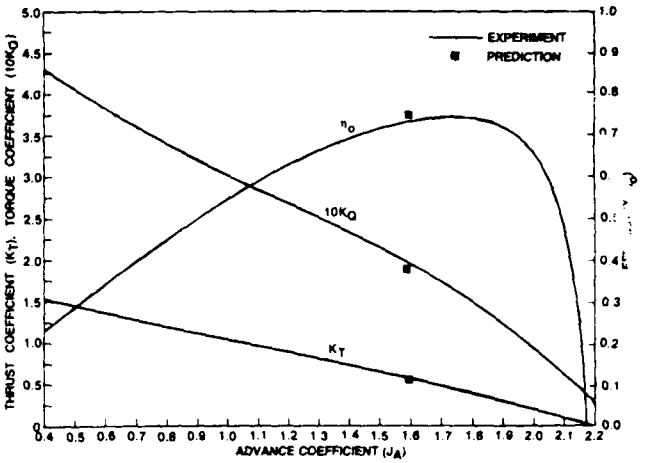

Fig. 8. CR propeller open–water test results and performance prediction.

torque prediction is 3.0 percent lower. The predicted thrust-ratio is 5.6 percent higher than the measurement and the torque-ratio prediction is almost equal to the experimental measurement. The predicted efficiency is 3.0 percent higher than that from the experiment. Overall the predicted values agree very well with the experimental measurements, and in general are within the accepted accuracy of the experimental measurements.

CONCLUSIONS AND RECOMMENDATIONS

The conclusions from this study are as follows:

1) The present design methodology is adequate for CR propellers in uniform flow, and
2) For moderate propeller loadings, the interaction velocities from lifting-line therory are adequate for use in the lifting-surface design.

There are several recommendations for future work on this topic:

1) Hull-propulsor interaction and effective wake: A methodology for calculating hull-propulsor interactions for CR pro-

pellers needs to be developed, including thrust deduction, wake fraction, and effective wake. This is particularly important for the aft propeller because of the complex interactions between the forward propeller and the hull, and between the two propellers.

2) Cavitation and unsteady forces: A methodology which can handle the unsteady circumferential variations of the mutual interaction velocities between the two propellers needs to be developed. Once developed, these unsteady velocities need to be incorporated into the cavitation and unsteady force calculations for the aft propeller.

ACKNOWLEDGMENTS

Funding for this work was provided by Office of Naval Technology under the Surface Ship Technology Program, Program Element 62121N. The authors would like to thank Dr. Bruce Cox of HRA for his helpful suggestions during this study, and Mr. Chris Kerr for preparing the graphics of the CR propeller set.

REFERENCES

Caster, E. B. and T. A. LaFone. 1975. A Computer Program for the Preliminary Design of Contrarotating Propellers. DTNSRDC Rpt. SPD-596-01, 141+xi p.

Caster, E. B., J. A. Diskin, and T. A. LaFone. 1975. A Lifting Line Computer Program for Preliminary Design of Propellers. DTNSRDC Rpt. SPD-595-01, 143 p.

Cebeci, T. 1978. A Computer Program for Calculating Incompressible Laminar and Turbulent Boundary Layers on Plane and Axisymmetric Bodies with Surface Roughness. California State University at Long Beach, Dept. of Mechanical Engineering, Report TR-78-1, 14 p.

Chen, B. Y-H. and A. M. Reed. 1988. A Lifting-Surface Program for Contrarotating Propellers. Symposium on Hydrodynamic Performance Enhancement for Marine Applications, NUSC, Newport, RI, pp 57–68

Chen, B. Y-H., A. M. Reed, and K-H. Kim. 1988. A Vane Wheel Propulsor for Naval Auxiliary. Symposium on Hydrodynamic Performance Enhancement for Marine Applications, NUSC, Newport, RI, pp 199–205.

Cox, B. D. and A. M. Reed. 1988. Contrarotating Propellers—Design Theory and Applications, SNAME Propellers '88 Symposium, Virginia Beach, VA, pp 15-1–15-29.

Greeley, D. S. and J. E. Kerwin. 1982. Numerical Methods for Propeller Design and Analysis in Steady Flow. *Trans SNAME*, 90:415–53.

Gunsteren, L. A. van. 1971. Application of Momentum Theory in Counterrotating Propeller Design. *Int. Shipbuilding Progress*, 18(206)359–72.

Kerwin, J. E., W. B. Coney, and C-Y. Hsin. 1986. Optimum Circulation Distributions for Single and Multi-Component Propulsors. *Twenty-First American Towing Tank Conference*, National Academy Press, pp 53–62.

Lee, J-T. 1987. A potential Based Panel Method for the Analysis of Marine Propellers in Steady Flow. MIT, Department of Ocean Engineering, Report 87-13, 150 p.

Lerbs, H. W. 1952. Moderately Loaded Propellers with a Finite Number of Blades and an Arbitrary Distribution of Circulation. *Trans SNAME*, 60:75–123.

———. 1955. Contra-Rotating Optimum Propellers Operating in a Radially Non-Uniform Wake. DTMB Rpt. 941, 28+ii p.

McCormick, B. W., Jr. 1953. Propeller Design Procedures. Penn State University, Ordinance Research Laboratory Technical Memorandum, TM 5.2400-22, 34 p.

Morgan, W. B. 1960. The Design of Counterrotating Propellers Using Lerbs' Theory. *Trans SNAME*, 68:6–38.

Naiman, I. 1943. Method of Calculating Performance of Dual-Rotating Propellers from Airfoil Characteristics. NACA Wartime Rpt. L-330, 41 p.

Nelson, D. M. 1972, Development and Application of a Lifting-Surface Design Method for Counterrotating Propellers. NUC Rpt. NUC TP-326, 23 p.

———. 1975. A Computer Program Package for Designing Wake-Adapted Counterrotating Propellers: A User's Manual. NUC Rpt. NUC TP 494, 254+iv p.

Theodorsen, T. 1944a. The Theory of Propellers: I—Determination of the Circulation Function and the Mass Coefficient for Dual-Rotating Propellers. NACA Rpt. 775, pp 35–51.

———. 1944b. The Theory of Propellers: IV—Thrust, Energy, and Efficiency Formulas for Single- and Dual-Rotating Propellers with Ideal Circulation Distribution. NACA Rpt. 778, pp 99–105.

Wang, M. H. 1985. Hub Effects in Propeller Design and Analysis. MIT, Department of Ocean Engineering, Rpt. 85-14, 191 p.

APPENDIX

Parametric Studies

The purpose of this study is to secure an optimum design for a CR propeller through parametric studies. In order to provide a fair comparison, a parametric study for a single rotation propeller was also carried out. The following range of single rotation propeller geometric characteristics were explored:

- propeller diameter, D, 5.8–7.6 m
- propeller rotational speed, N, 40–100 rpm.

The parametric studies for the single rotation propeller in uniform flow were performed with a fixed blade number, Z, of 7. As is shown in Figure 9, the larger the propeller diameter, the higher the efficiency which can be achieved because of reduced the propeller blade loading. It can be observed that the optimum rotational speed is about 80 rpm when the corresponding propeller diameter is 6.10 meters.

The CR propeller parametric studies covered the following range of parameters:

- Forward propeller diameter, D_f, 5.8–7.6 m
- Forward propeller rotational speed, N_f, 20–70 rpm
- Ratio of propeller diameters, D_a/D_f, 0.80–0.95
- Ratio of rotational speeds, N_a/N_f, 0.8–1.2
- Axial spacing, x/D_f, 0.15–1.0

Although the forward propeller diameter and rotational speed for this particular design have been given as 6.10 meters and 51 rpm, respectively; the parametric studies include these variables to validate the selection of these specific values.

Propeller Diameter: A parametric study was executed to determine the highest efficiency for a range of forward propeller diameters. The ratios of the propeller diameter and rotational speed of the aft propeller to those of the forward propeller were designated as 0.85 and 1.0, respectively. The axial spacing was chosen to be 0.25 of the forward propeller diameter.

Figure 10 shows that the larger the forward propeller diameter, the higher the efficiency which is obtained. It can be seen that the CR propeller is more efficient than the single rotation propeller with the same diameter, because the aft propeller of the CR propeller set recovers the rotational energy in the slipstream and both propellers have lighter blade loadings.

Ratio of Propeller Diameters: A parametric study was carried out to determine the effect of the ratio of diameters between the two propellers. The ratio of the rotational speed is equal to 1.0 and the axial spacing is 0.25 of the forward propeller diameter.

Figure 11 shows that there is an optimum aft propeller diameter at which the CR propeller gains the highest efficiency. In general, as the aft propeller diameter increases, there is more mass flow into the propeller disk which results in reduced propeller blade loading and higher efficiency. However, if the aft propeller diameter is larger than the radius of the forward propeller wake, the efficiency drops because blade drag increases without recovering additional rotational energy. Since this study does not account for mass conservation between the two propellers, the aft propeller diameter can not be determined solely based on this study, but rather mass conservation must also be satisfied.

Ratio of Rotational Speeds: The effect of the ratio of the rotational speeds on efficiency is shown in Figure 12. The ratio of the propeller diameters is 0.85 and the axial spacing is 0.25 of the forward propeller diameter. It indicates that there is no significant change in propeller efficiency over rotational speed ratios between 0.8 and 1.2.

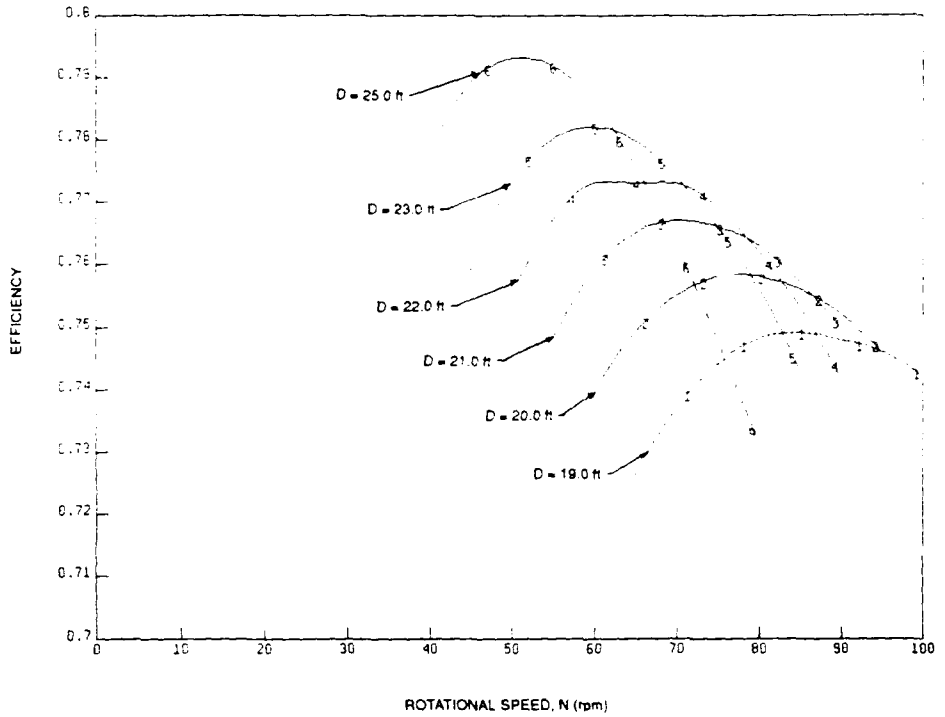

Fig. 9. Propeller efficiency versus rotational speed with various propeller diameters for a single rotation propeller.

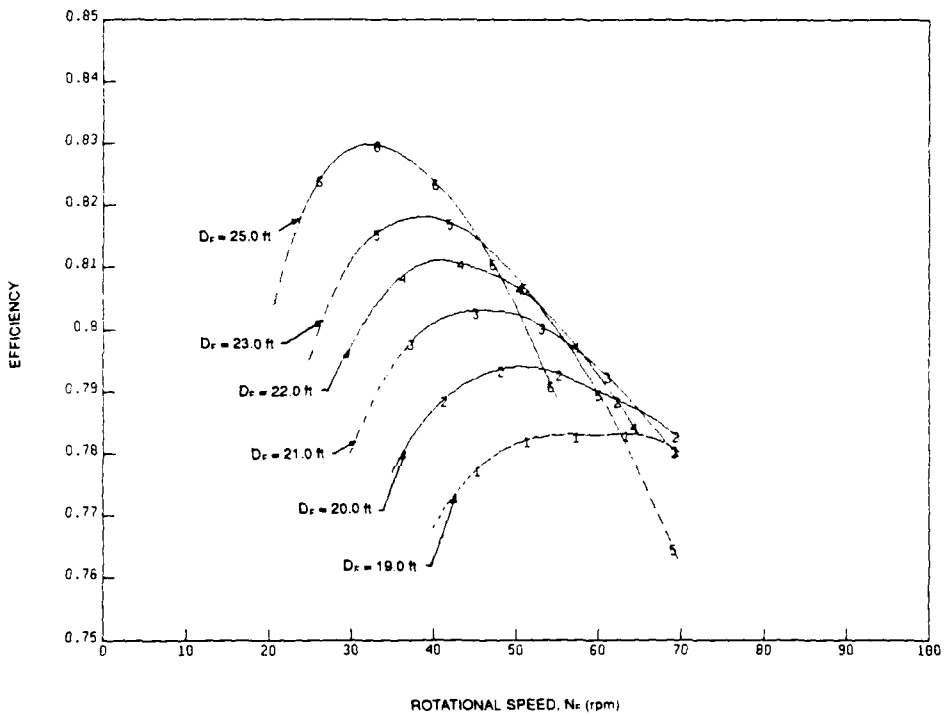

Fig. 10. Propeller efficiency versus rotational speed with various forward propeller diameters for a CR propeller.

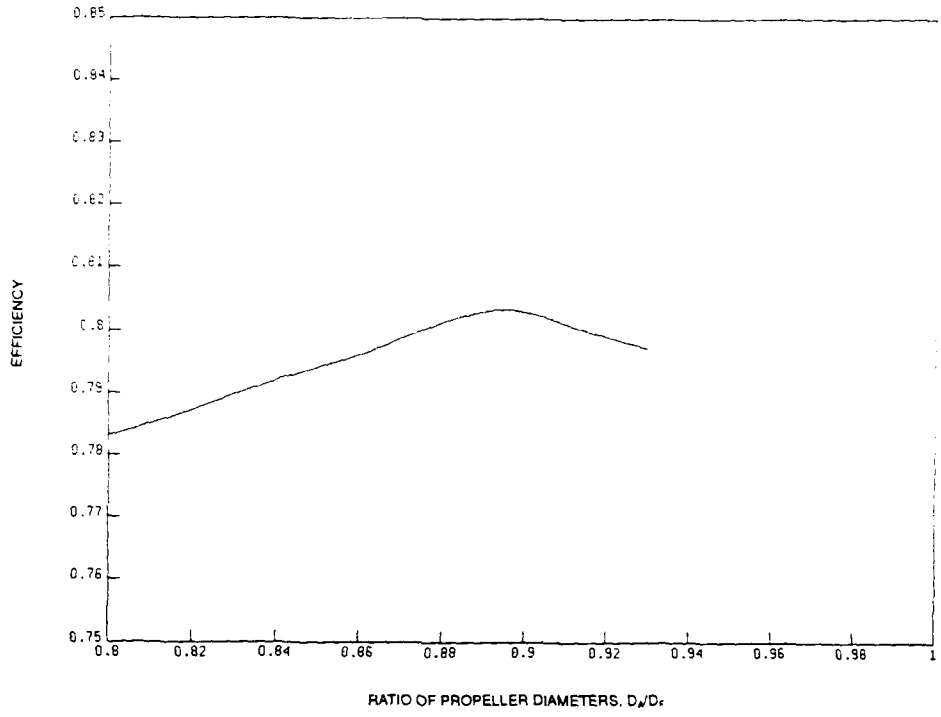

Fig. 11. Propeller efficiency versus ratio of propeller diameter for fixed ratio of rotational speed and axial spacing.

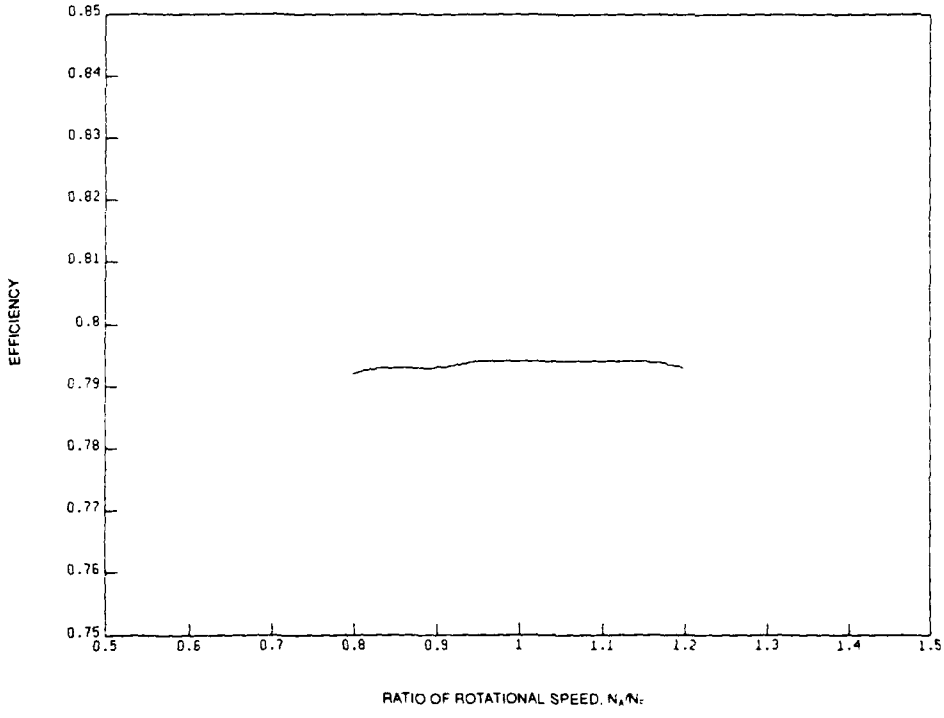

Fig. 12. Propeller efficiency versus ratio of rotational speed for fixed ratio of propeller diameter and axial spacing.

Axial Spacing: Figure 13 shows the effect of the axial spacing between the forward and aft propellers. The ratios of propeller diameters and rotational speeds are 0.85 and 1.0, respectively. The calculations indicate that the CR propeller efficiency is almost constant as the axial spacing is varied between 0.15 and 1.0 times the forward propeller diameter.

Hydrodynamic Pitch: The radial distributions of the hydrodynamic pitch, $\pi r \tan \beta_i$, corresponding to both the optimum and the unloaded circulation distributions on the forward and aft propellers are shown in Figures 14 and 15, respectively. Figure 14 shows that the $\pi r \tan \beta_i$ corresponding to the unloaded circulation distribution for the forward propeller is reduced substantially near the hub. On the other hand, Figure 15 shows that the $\pi r \tan \beta_i$ of the aft propeller changes little near the hub due to reduced circulation. This is mainly due to the fact that the self-induced tangential velocity of the aft propeller and the tangential velocity induced by the forward propeller at the aft propeller cancel each other, even though both of the distributions have reduced circulation at the hub. Hence, the net tangential induced velocity at the aft propeller changes little between the optimum and the unloaded cases. It is not believed that the extreme reduction in $\pi r \tan \beta_i$ near the tip of the aft propeller is realistic. This extreme reduction in $\pi r \tan \beta_i$ may be caused by the sensitivity of the numerical scheme in the lifting-line program to the shape of the circulation distribution.

The blade pitch distribution from lifting-surface calculations using the unloaded circulation distributions are also shown in Figures 14 and 15. These figures indicate that the blade pitch and $\pi r \tan \beta_i$ for the unloaded circulation distribution are very similar. In contrast to the $\pi r \tan \beta_i$ distribution corresponding to the optimum circulation distribution, the pitch of the forward propeller is reduced near both the hub and tip. For the aft propeller, Figure 15 indicates that relative to the $\pi r \tan \beta_i$ distribution corresponding to the unloaded circulation distribution, the pitch is reduced near the tip, however, not near the hub.

The lifting-surface code was also used to calculate the pitch distribution for the optimum circulation distribution for the aft propeller. It is found that the unloaded pitch is reduced relative to the optimum pitch near the hub. A lesson learned from this is that lifting-line or lifting-surface results should be compared separately rather than with each other, especially in CR propeller design.

Wake Behind Forward Propeller: In order to confirm that the CR propeller improves the propeller efficiency, calculations of the axial and tangential induced velocities were carried out. They were calculated at 0.25 of the forward propeller diameter behind the forward propeller reference line (i.e. at the aft propeller reference line) with and without the presence of the aft propeller. Figure 16 shows that the axial induced velocity is substantially increased by the presence of the aft propeller. This indicates that the aft propeller increases the mass flow and results in a decrease in the propeller loading. Figure 17 shows that the aft propeller decreases the total tangential induced velocity. This shows that the energy losses in the slipstream due to tangential velocity are successfully reduced by the CR set.

Geometric specification: The chord distributions which were chosen for the forward and aft propellers are shown in Figure 18. The expanded area ratio (EAR) was calculated based on both Burrill's and Keller's criteria for cavitation inception. Figure 19 shows the thickness distributions for the forward and aft propellers. The skew distribution is given in Figure 20. There was no total rake for either propeller. The stress distributions corresponding to these choices of geometry are given in Figure 21.

Performance Prediction

Steady force predictions for design and off-design conditions were made using the inverse lifting-surface code (PSF-2) and panel code (PSF-10) described earlier. The input

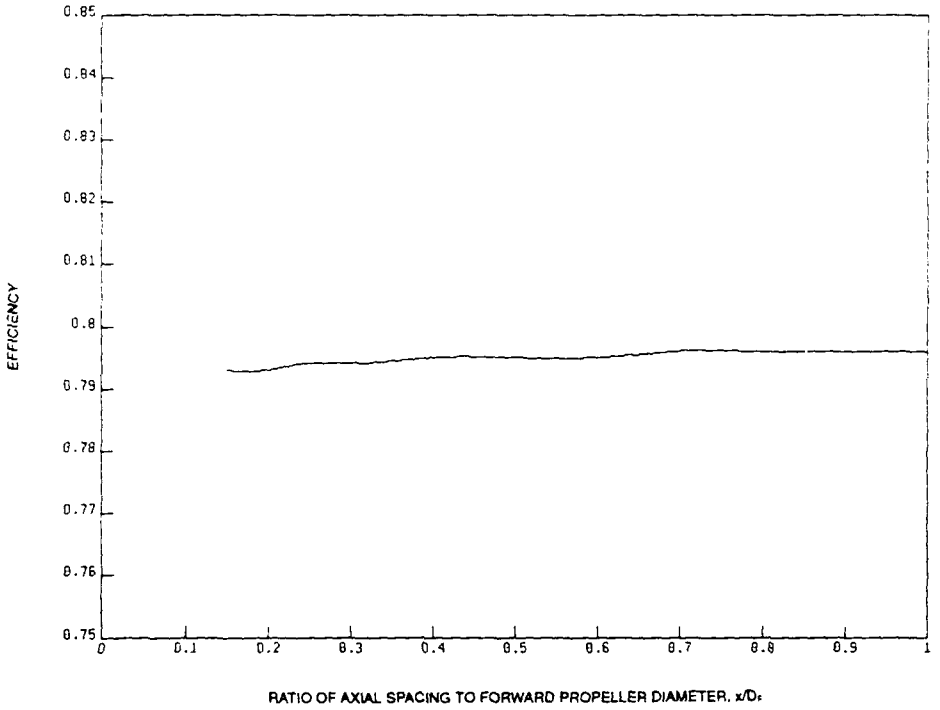

Fig. 13. Propeller efficiency versus axial spacing to forward propeller diameter for fixed ratios of propeller diameter and rotational speed.

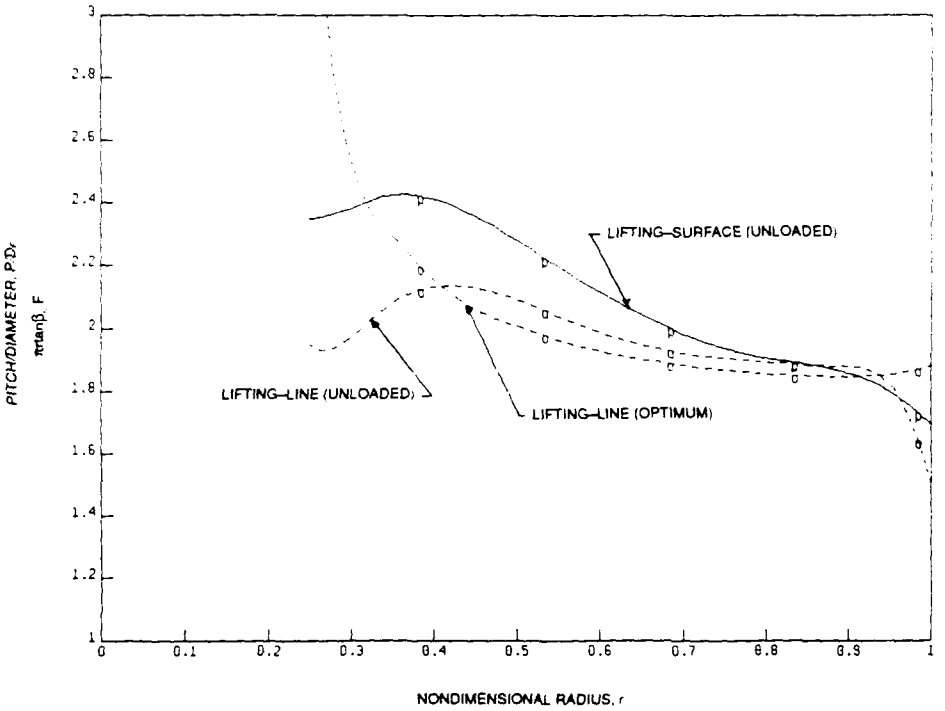

Fig. 14. *Radial distribution of optimum and unloaded* $\pi r \tan\beta_i$ *and unloaded pitch to diameter ratio for forward propeller.*

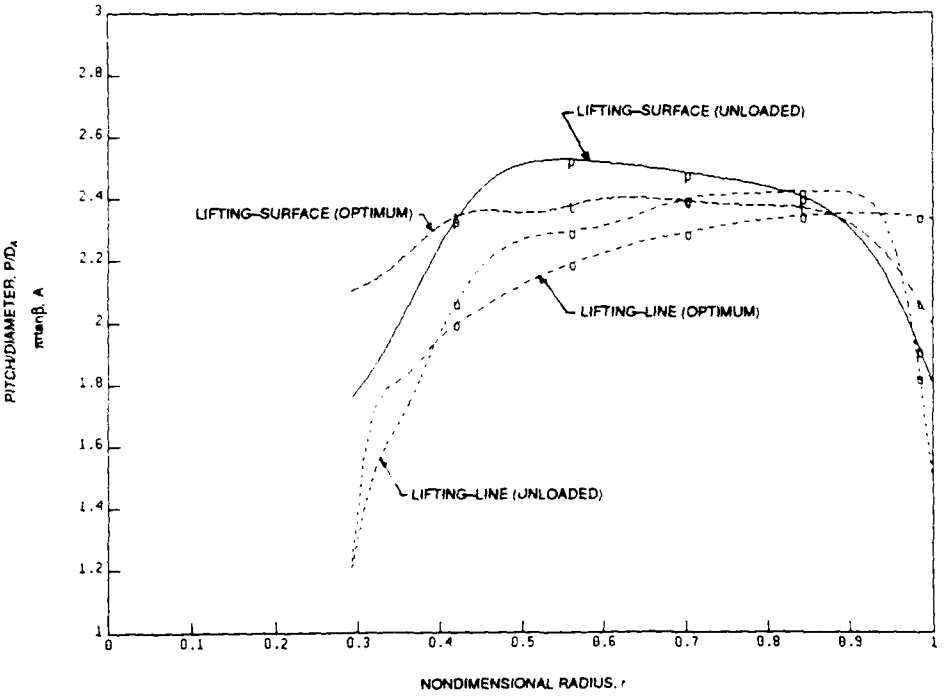

Fig. 15. Radial distribution of optimum and unloaded $\pi r \tan\beta_i$ and pitch to diameter ratio for aft propeller.

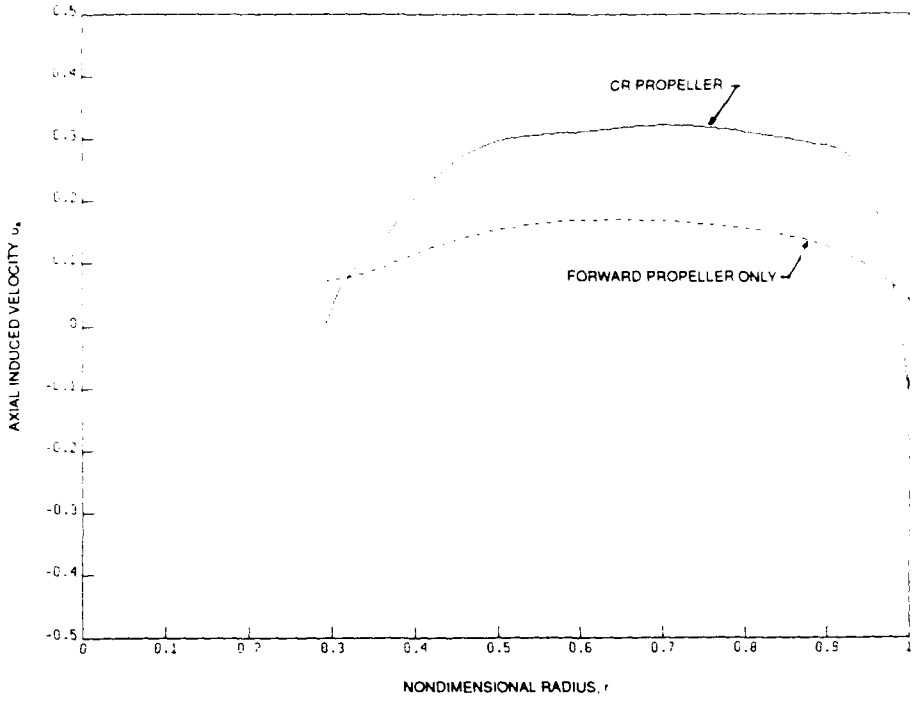

Fig. 16. Radial distribution of axial induced velocity with and without aft propeller calculated at 0.25 D_F behind the forward propeller.

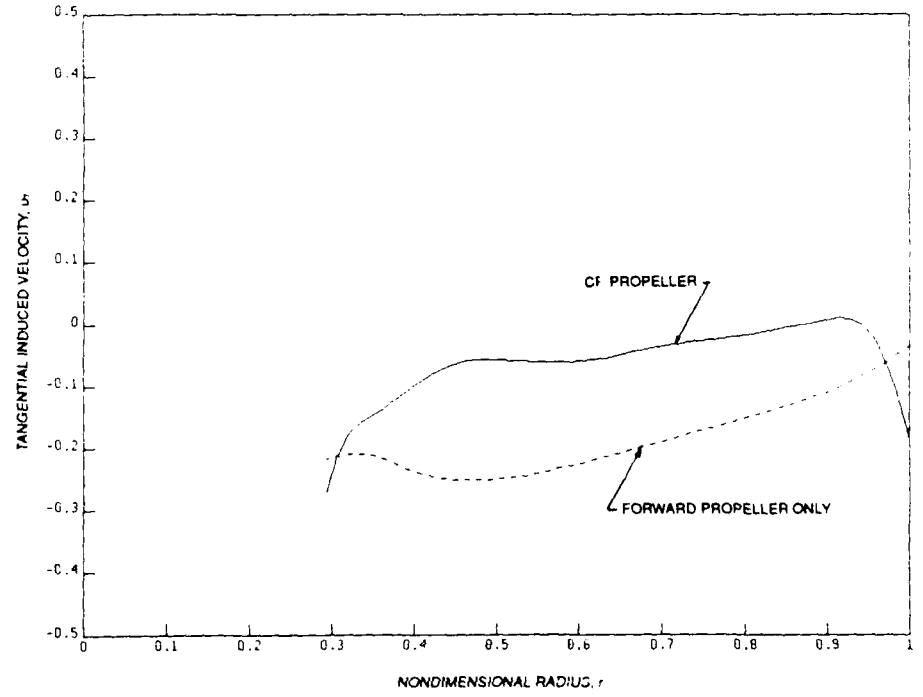

Fig. 17. Radial distribution of tangential induced velocity with and without aft propeller calculated at 0.25 D_F behind the forward propeller.

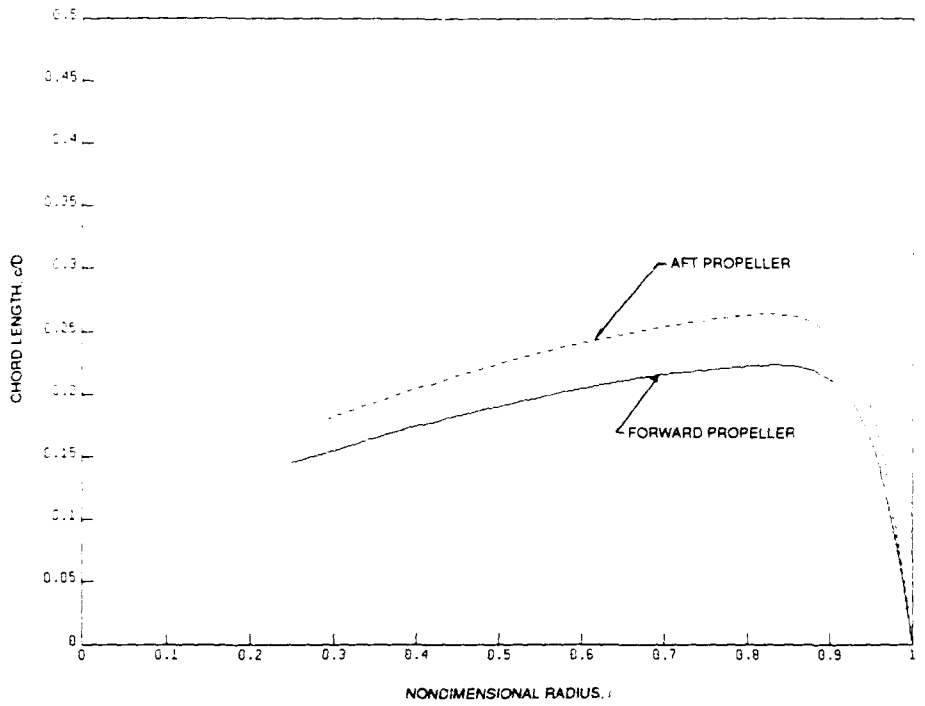

Fig. 18. Radial distribution of chord length.

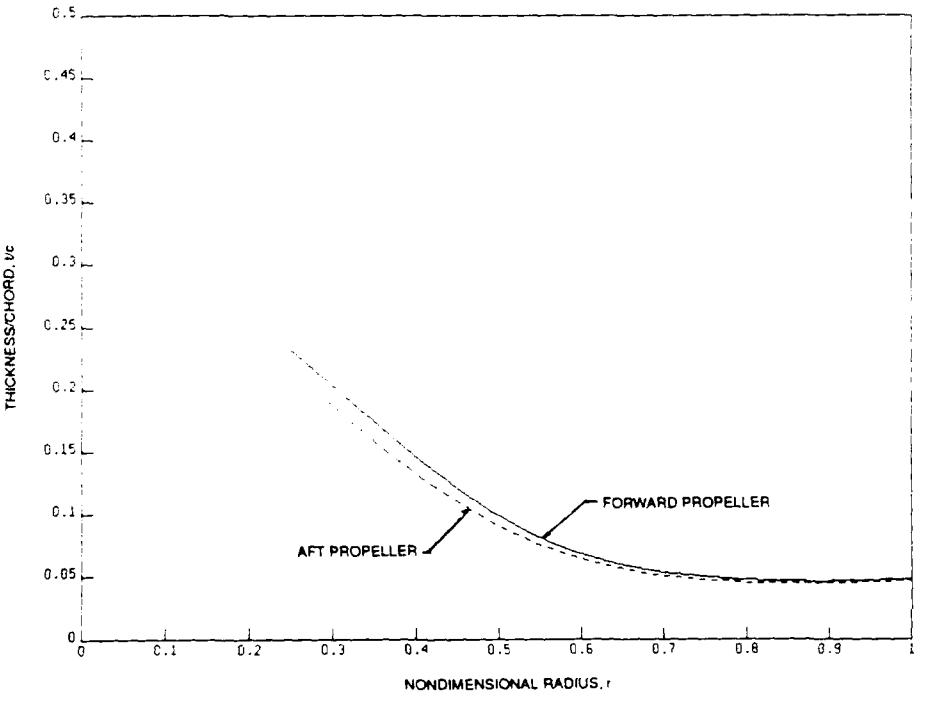

Fig. 19. Radial distribution of thickness.

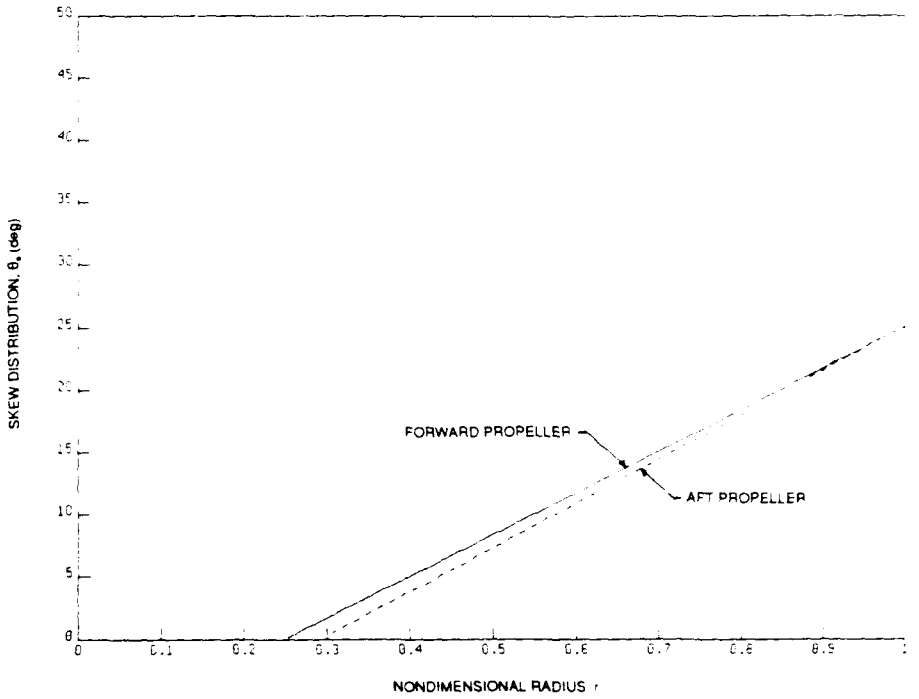

Fig. 20. Radial distribution of skew.

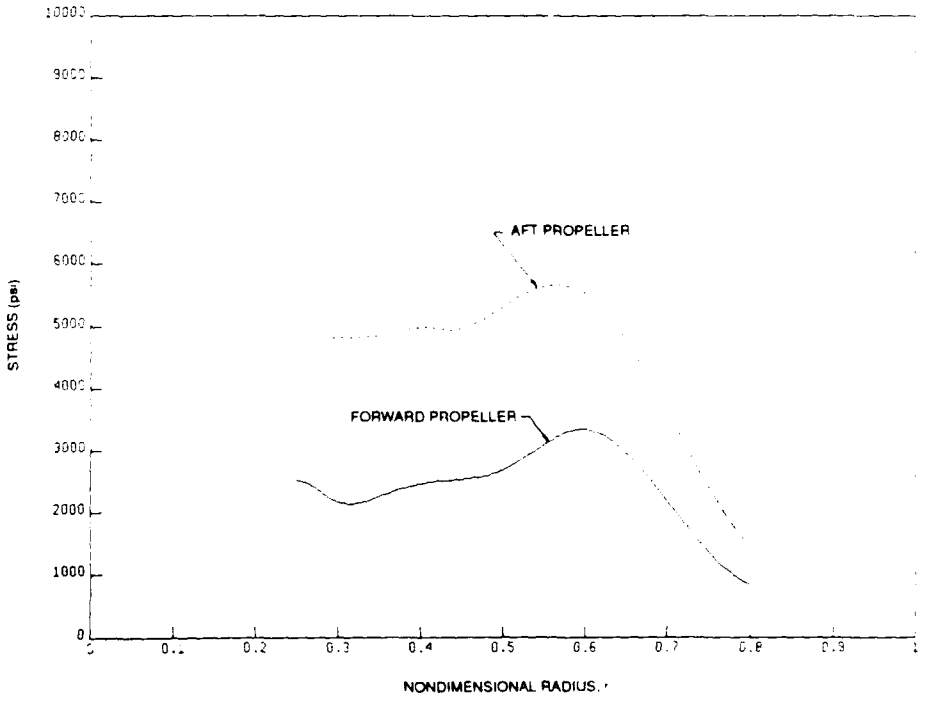

Fig. 21. Radial distribution of stress.

to PSF-2 and PSF-10, the blade geometry and the wake, are directly inherited from the output of the lifting-surface design code, PBD-11. While PSF-2 does not account for hub effects, PSF-10 can account for presence of a hub.

A combination of the design (PBD-10) and the analysis (PSF-2) codes has been used and tested for single screw propellers for several years. The results show that the thrust and torque predictions from these codes agree well with experiments. In the present study, the combination of the design (PBD-11) and the analysis (PSF-10) codes with hub effects are evaluated. Using PSF-2 as a reference, a comparison of the circulation distribution, an input to the design code and an output from the analysis code, is given.

For the forward propeller, Figure 22 shows that the circulation distribution predicted by PSF-10 without a hub is higher near the hub and lower near the tip than that of PSF-2. Figure 23 shows a comparison of the circulation distribution between PSF-10 with a hub and the input to PBD-11. This comparison shows that PSF-10 agrees well with PBD-11 near the tip but predicts slightly higher circulation than was input to PBD-11 near the hub. A comparison of Figures 22 and 23 also shows that because they don't account for hub effects, both PSF-2 and PSF-10 without a hub predict lower circulation near the hub than was input to PBD-11.

As shown in Table 3, the thrust and torque predictions from PSF-10 without a hub are almost identical to those from PSF-2. However, PSF-10 with a hub predicts 5.4 percent higher thrust and 3.1 percent higher torque than PSF-2. The thrust prediction from PSF-10 with a hub is 4.1 percent higher than the design value (from PBD-11), while the torque prediction is almost identical to the design prediction.

For the aft propeller, Figure 24 shows that PSF-10 without a hub has the same trend as Figure 22 does for the forward propeller. Figure 25 shows that PSF-10 with a hub has lower circulation near the tip and higher circulation near the hub than was input to PBD-11.

The thrust predicted for the aft propeller by PSF-10 without a hub is 4.9 percent lower than that predicted by PSF-2, while the torque prediction is almost identical to that of PSF-2. The thrust prediction from PSF-10 with the hub is only 1.2 percent higher than that from PSF-2, however, the torque prediction is 7.9 percent higher. The thrust prediction from PSF-10 with a hub is 4.6 percent lower than the design prediction (from PBD-11). Nonetheless, the torque prediction is 1.3 percent higher than the design prediction.

The thrust ratio predicted by PSF-10 with a hub is 9.0 percent higher than the design value while the prediction of the total thrust is 0.9 percent lower than the design value. In addition, the predicted torque ratio is very close to the design value. PSF-10 predicts that the total net blade circulation at the blade root for the forward and aft propellers together is almost zero, so the hub vortex should be negligable.

Final CR propeller geometry

The final geometric specifications of the CR propeller, including the details of the leading and trailing edges were computed using the computer code, XYZ-PROP, developed by Brockett.* All the input data such as, the chord length, thickness, skew, pitch and camber distributions were faired by a cubic spline procedure before being input to XYZ-PROP. A list of the chord length, thickness, skew, pitch and camber distributions are given in Table 4.

* Brockett, T. E. 1976. Analytical Specification of Propeller Blade-Surface Geometry. DTRC Ship Hydrodynamics Department Report, DTRC/SHD-699-01.

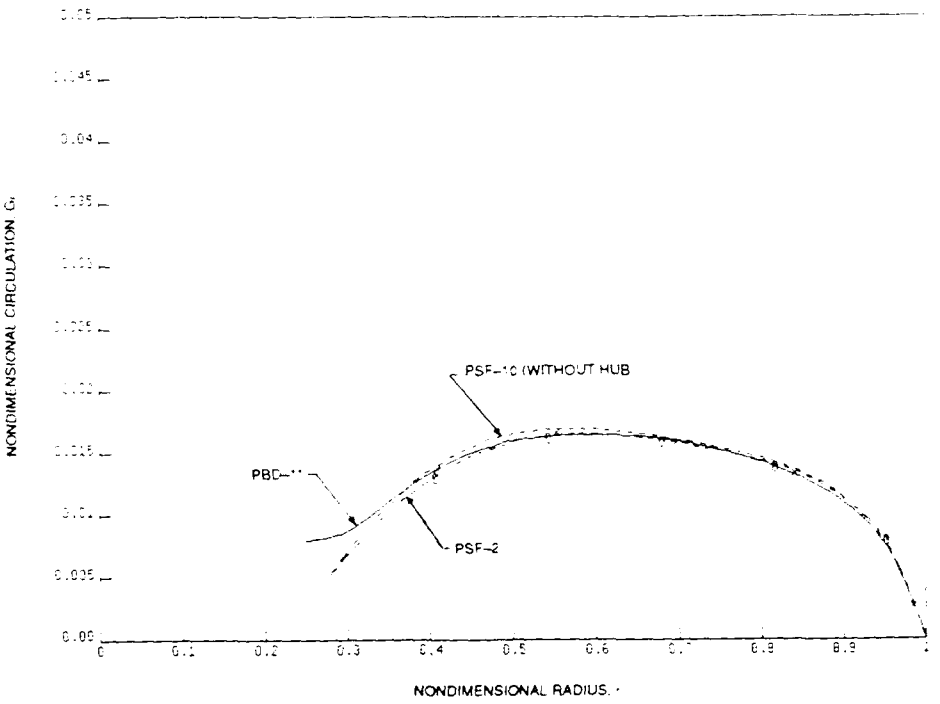

Fig. 22. Circulation distribution from PSF–2, PSF–10 without hub option and PBD–11 for forward propeller.

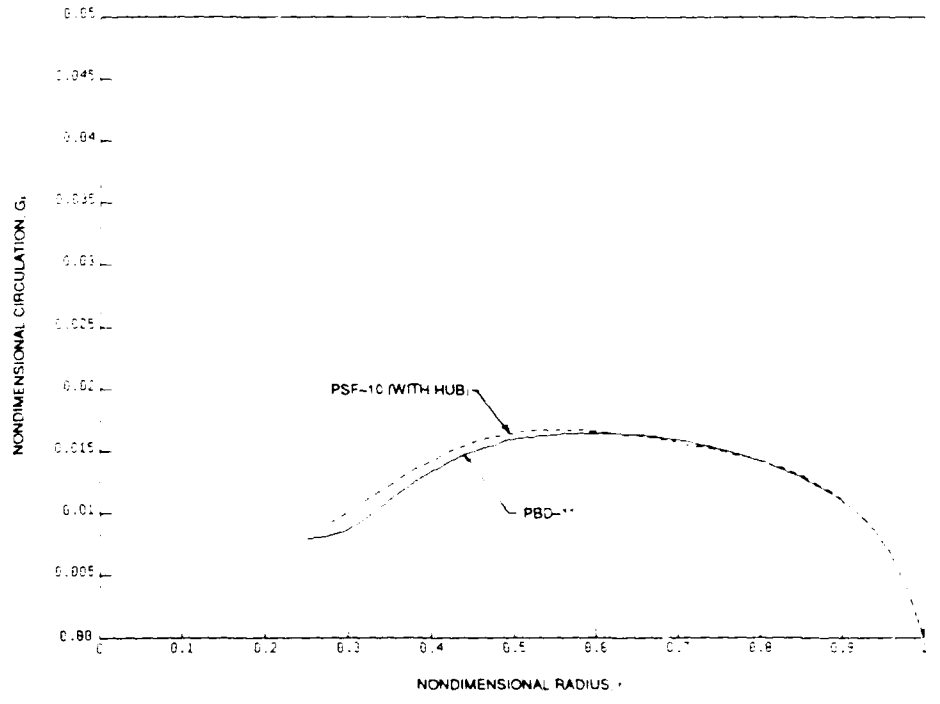

Fig. 23. Circulation distribution from PSF–10 with hub option and PBD–11 for forward propeller.

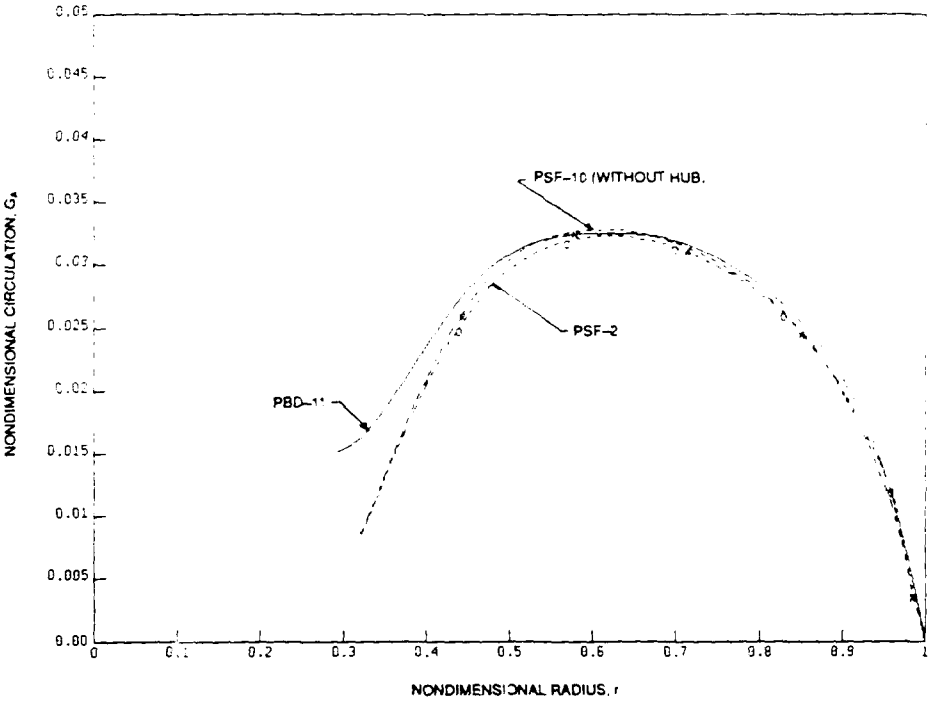

Fig. 24. Circulation distribution from PSF–2, PSF–10 without hub option and PBD–11 for aft propeller.

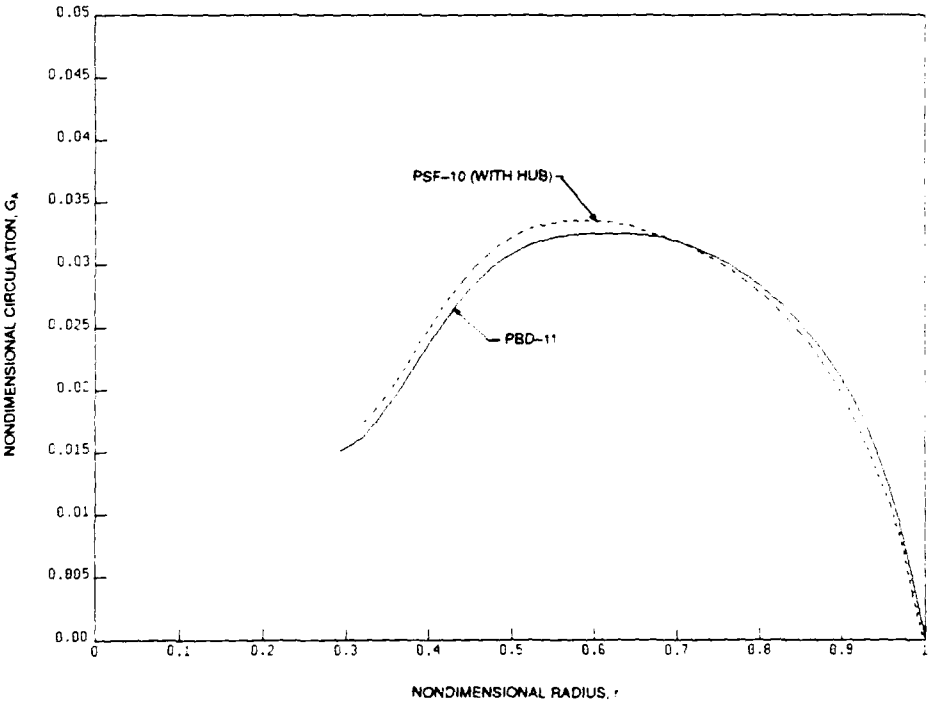

Fig. 25. Circulation distribution from PSF–10 with hub option and PBD–11 for aft propeller.

Table 3. Performance prediction for CR propeller.

Forward Propeller	K_T	K_Q	N(rpm)
PSF-2	0.2913	0.0964	51
PSF-10 (w/o hub)	0.2940	0.0970	51
(with hub)	0.3070	0.0995	51

Aft Propeller	K_T	K_Q	N(rpm)
PSF-2	0.2646	0.0863	51
PSF-10 (w/o hub)	0.2516	0.0868	51
(with hub)	0.2678	0.0931	51

CR Propeller Set	T_F/T_A	Q_F/Q_A	N_F/N_A	Efficiency
PSF-2	1.100	1.117	1.0	0.770
PSF-10 (w/o hub)	1.168	1.117	1.0	0.751
(with hub)	1.146	1.068	1.0	0.755

Note: The coefficients for aft propeller are based on forward propeller diameter.

Table 4. Final design geometry for CR propeller.

(a) Forward Propeller

r	c/D	P/D	i_T/D	θ_s	t/c	f_m/c
0.250000	0.145500	2.34700	0.0000	0.000000	0.231810	0.008152
0.275000	0.150082	2.35867	0.0000	0.833401	0.217406	0.013073
0.300000	0.154800	2.38000	0.0000	1.666720	0.203000	0.017704
0.350000	0.164200	2.42300	0.0000	3.333350	0.174340	0.024782
0.400000	0.173250	2.41150	0.0000	5.000000	0.146600	0.028885
0.500000	0.189800	2.28010	0.0000	8.333300	0.099100	0.030105
0.600000	0.203800	2.11450	0.0000	11.666700	0.068090	0.025915
0.700000	0.214900	1.98000	0.0000	15.000000	0.053530	0.021684
0.800000	0.222600	1.90300	0.0000	18.333300	0.047500	0.019012
0.900000	0.212000	1.85690	0.0000	21.666600	0.046030	0.019200
0.950000	0.164200	1.79760	0.0000	23.333300	0.046700	0.020800
1.000000	0.000000	1.68930	0.0000	25.000000	0.047770	0.019200

(b) Aft Propeller

r	c/D	P/D	i_T/D	θ_s	t/c	f_m/c
0.294100	0.180181	1.75980	0.0000	0.000000	0.190747	−0.008100
0.300000	0.181508	1.77800	0.0000	0.208950	0.187310	−0.005600
0.320000	0.186084	1.85020	0.0000	0.917261	0.175764	0.003400
0.350000	0.193000	1.98500	0.0000	1.979740	0.158957	0.017200
0.400000	0.204070	2.24000	0.0000	3.750530	0.133036	0.037200
0.450000	0.214380	2.43000	0.0000	5.521320	0.110136	0.049300
0.500000	0.223900	2.51000	0.0000	7.292110	0.090832	0.050100
0.600000	0.240500	2.51800	0.0000	10.833690	0.064055	0.044500
0.700000	0.253600	2.48540	0.0000	14.375270	0.050651	0.039150
0.800000	0.262500	2.43800	0.0000	17.916840	0.045210	0.035300
0.900000	0.248900	2.31000	0.0000	21.458420	0.044422	0.033200
0.950000	0.193400	2.12570	0.0000	23.229210	0.045318	0.033700
1.000000	0.000000	1.80000	0.0000	25.000000	0.046695	0.038700

THIS PAGE INTENTIONALLY LEFT BLANK

INITIAL DISTRIBUTION

Copies	
1	Army Chief of Res & Dev
1	AER&DL
4	CHONR
	1 Lib
	1 Code 11
	1 Code 21
	1 Code 12
4	ONR Boston
4	ONR Chicago
4	ONR London, England
1	NRL
2	USNA
	1 Lib
	1 Johnson
1	NAVPGSCOL Lib
1	NROTC & NAVADMINU, MIT
1	NADC
4	NOSC
	1 1311 Lib
	1 6005
	1 13111 Lib
	1 Mautner
1	NSWC
31	NAVSEA
	5 SEA 05R
	1 SEA 55
	3 SEA 55N
	1 SEA 55W
	3 SEA 56D
	1 SEA 56X
	3 SEA 56X1
	1 SEA 56X2
	3 SEA 56X7
	1 SEA 56X5

Copies	
	NAVSEA (Continued)
	1 SEA 56XN
	1 PMS-383
	1 PMS-392
	1 PMS-396
	1 PMS-399
	1 PMS-400
	1 SEA Tech Rep Bath, England
	2 DET Norfolk (Sec 6660)
2	MMA
	1 Lib
	1 Maritime Res Cen
12	DTIC
2	HQS COGARD
1	US Coast Guard (G-ENE-4A)
1	LC/SCI & Tech Div
2	NASA STIF
	1 Dir Res
1	NSF Engr Div/Lib
1	DOT Lib
2	U. Cal Berkeley/Dept Name
	1 Name Lib
	1 Webster
1	U. Mississippi Dept of M.E.
	1 Fox
3	CIT
	1 AERO Lib
	1 Acosta
	1 Wu
4	U. Iowa
	1 Lib
	1 IHR/Kennedy
	1 IHR/Stern
	1 IHR/Patel

INITIAL DISTRIBUTION (Continued)

Copies	
3	U. Michigan/Dept Name 1 Name Lib 1 Parsons 1 Vorus
3	MIT 1 Barker Engr Lib 2 Ocean Engr/Kerwin
3	State U Maritime Coll 1 ARL Lib 1 Engr Dept 1 Inst Math Sci
4	Penn State U ARL 1 Lib 1 Henderson 1 Gearhart 1 Thompson
1	Boeing Adv Amr Sys Div
1	BB&N/Jackson
1	Brewer Engr Lab
1	Cambridge Acous/Junger
1	Calspan, Inc/Ritter
1	Stanford U/Ashley
1	Stanford Res Inst Lib
2	Sit Davidson Lab 1 Lib 1 Savitski
1	Texas U ARL Lib
1	Utah State U/Jeppson
2	VPI/Dept Aero & Ocean Engr 1 Schetz 1 Kaplan
2	Webb Inst 1 Ward 1 Hadler

Copies	
1	WHOI Ocean Engr Dept
1	WPI Alden Hydr Lab Lib
1	ASME/Res Comm Info
1	ASNE
1	SNAME/Tech Lib
1	AERO Jet-General/Beckwith
1	Allis Chalmers, York, PA
1	AVCO Lycoming
1	Baker Manufacturing
1	Bird-Johnson Co/Norton
1	Douglas Aircraft/Lib
2	Exxon Res Div 1 Lib 1 Fitzgerald
1	Friede & Goldman Michel
1	General Dynamics, EB/Boatwright
1	Gibbs & Cox/Lib
1	Rosenblatt & Son/Lib
1	Grumman Aerospace/Carl
1	Tracor Hydronautics/Lib
1	Ingalls Shipbuilding
1	Inst for Defense Anal
1	Itek Vidya
1	Lips Duran/Kress
1	Littleton R & Engr Corp/Reed

INITIAL DISTRIBUTION (Continued)

Copies	
1	Litton Industries
1	Lockheed, Sunnyvale/Waid
2	McDonnel Douglas, Long Beach 1 Cebeci 1 Hess
1	Maritech, Inc/Vassilopoulis
2	HRA, Inc 1 Cox 1 Scherer
1	Nielsen Engr/Spangler
1	NKF Associates/Noonan
1	NAR Space/Ujihara
2	Atlantic Applied Research 1 Brown 1 Greeley
1	Propulsion Dynamics, Inc
1	Sperry Sys Mgmt Lib/Shapiro
1	OF Technologies/Furuya
1	UA Hamilton Standard/ Cornell

CENTER DISTRIBUTION

Copies	Code	Name
1	0120	
1	12	
1	112.1	Nakonechny
1	15	W.B. Morgan
1	1506	Walden
1	1508	Boswell

CENTER DISTRIBUTION (Cont.)

Copies	Code	Name
1	152	Lin
1	1521	Day
1	1521	Karafiath
1	1521	Hurwitz
1	1522	Remmers
1	1522	Wilson
1	154	McCarthy
1	154.1	Yim
1	1542	Huang
20	1544	Chen
20	1544	Reed
1	156	Cieslowski
1	172	Krenzke
1	1720.6	Rockwell
1	19	Sevik
1	1901	Strasberg
1	1905	Blake
1	1906	Biancardi
1	1942	Mathews
1	1962	Silcullen
1	522.1	TIC (C)
1	522.2	TIC (A)
10	522.4	Reports Control